Integrated Nano, 2024, Vol. XX, No.XX

DOI: 10.62184/in.jin010120241

Research Article

SCIENCE PARK PUBLISHER

Integrated Nano

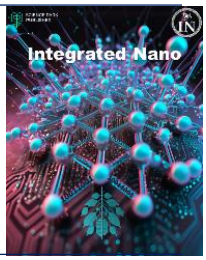


# Aluminum Oxide Nanoparticles as a Photocatalyst for Water Splitting

**Mai Medhat[1], Ahmed M. Elshaer[2], Moataz Soliman[1], Shaker Ebrahim[1], Marwa Khalil[3,*]**

[1] Materials Science Department, Institute of Graduate Studies and Research, Alexandria University, P.O. Box 832, Alexandria, Egypt

[2] Computer Engineering Department, Higher Institute of Engineering and Technology, Elbohaira, Egypt

[3]Composite and Nanostructured Materials Research Department, Advanced Technology and New Materials Research Institute, City of 6 Scientific Research and Technological Applications (SRTA-City), New Borg El Arab City, P.O. Box 21934 Alexandria, Egypt

**Received: 22, 12, 2023; Accepted: 25, 02, 2024; Published: 01, 04, 2024**



## Abstract

Among various photoinduced hydrogen gas production techniques, photochemical catalytic water splitting is promising and an ideal future energy source because of the low cost, stability, and high sustainability of the reaction system features. Aluminum oxide nanoparticles ($Al_2O_3$ NPs) as a photocatalyst for the splitting of water into hydrogen gas using solar energy is one of the noble missions of material science. In this work, pure aluminum oxide and L-methionine-capped aluminum oxide NPs have been synthesized using the sol-gel method. The pure $Al_2O_3$ and capped $Al_2O_3$ NPs with L-methionine were investigated by Fourier transform infrared (FTIR), X-ray diffractometer (XRD), high-resolution transmission electron microscopy (HRTEM), and Zeta potential. It was found that the average particle sizes of $Al_2O_3$ NPs and capped $Al_2O_3$ NPs with L-methionine were 13 and 20 nm, respectively. L-methionine-capped $Al_2O_3$ NPs had a higher negative charge with a potential of - 24.5 mV. The capping agent slightly improved the production of hydrogen from 44 to 60 ml at 75° C after 30 min under illumination.

**Keywords:** Aluminum oxide; Nanoparticles; L-methionine; Water splitting; Hydrogen production

## 1. Introduction

Research and technological development resort to various renewable/non-conventional energy resources become a need at present due to very high environmental impacts and limited stocks of conventional energy resources. It's predicted that hydrogen will play a key role in shifting the global energy system towards a sustainable energy system by 2050 [1-5]. Hydrogen sources are the hydrocarbons that are produced from fossil fuels [2, 3]. Many industries are using hydrogen such as a catalyst in petroleum processing and petrochemical production, oil and fat hydrogenation, using in fertilizer production, Raney nickel catalyst, oxygen scavenger, in addition as a fuel [6, 7].

The characteristics that make hydrogen the best energy carrier are: high efficiencies of production and conversion into electricity, completely renewable fuel; storage as a gas, liquid, or metal hydride that can easily be transported via pipelines or tankers over long distances; conversion into other forms of energy [1, 6]. The production processes of hydrogen are chemical, biological, electrolytic, thermo-chemical, photolytic, and splitting of water [8, 9].

Hydrogen is produced from the splitting of water through water electrolysis, alkaline electrolysis, polymer electrolyte membrane electrolysis, photocatalysis, photo-biological production, high-temperature water decomposition, and thermo-chemical [10, 11]. Photocatalytic water splitting reactions are

DOI: 10.62184/in.jin010120241

Research Article

categorized into two types: photoelectrochemical and photochemical. Although the underlying principles of photochemical and photoelectrochemical systems are similar, their structural arrangements vary [12]. The difference is that both hydrogen evolution reaction and oxygen evolution reaction half-reactions happen in the suspending photocatalyst particles in the suspension system, resulting in the evolution of a mixture of oxygen and hydrogen. In contrast, water redox reactions in the photoelectrochemical system are performed on two different surfaces (photoanode and photocathode) respectively, which to a large extent simplifies the subsequent gas separation process and promotes the engineering production of hydrogen or oxygen [13, 14]. Photochemical reactions use a semiconductor material that absorbs photons with energies greater than their bandgap energy and light energy is directly used to execute the chemical reaction [10, 12]. In photochemical reactions, the factors that affect the reaction behavior of hydrogen production are crystal structure, operating temperature, bandgap, light intensity, and the pH of the solution. Several essential conditions must be met for the Photochemical water splitting process: (1) strong light absorption; (2) rapid charge separation; (3) low redox potential; and (4) acceptable stability. To now, researchers from several fields throughout the world are investigating novel material systems that meet all of these characteristics [15]. Titanium dioxide is the most common semiconductor used in hydrogen production, however, $TiO_2$ has rapid recombination of photogenerated electron-hole pairs, wide bandgap limits $TiO_2$ use in the visible light region, and large over the potential for hydrogen evolution on $TiO_2$ surface [16-18].

Valery Rosenband et al. presented a parametric investigation of aluminum water reaction to generate hydrogen, using a novel activated aluminum powder. An initial thermo-chemical process involving a small fraction of a lithium-based activator induced a spontaneous reaction of the activated aluminum particles with water [19, 20]. This work aims to generate hydrogen gas by $Al_2O_3$ NPs. The advantage and the novelty of $Al_2O_3$ NPs can be used in visible light. Also, it has a high absorption capacity, non-toxic, highly abrasive, thermally stable, and inexpensive. Adding L-methionine as a capping agent improves the properties of $Al_2O_3$ NPs and provides high hydrogen gas yields more than pure $Al_2O_3$.

## 2. Materials and Methods

### 2.1. Materials

Ethanol (95%) was received from Carlo ERBA Reagents Spain. Ammonia solution (28%) was purchased from Chem Solute Germany, L-methionine was supplied by Bio Basic Canada INC. Aluminum chloride hexahydrate was bought from Panreac Quimica SA Barcelona.

### 2.2. Preparations of $Al_2O_3$ NPs

An ethanolic solution of 0.1 M $AlCl_3.6H_2O$ was prepared by adding 150 ml of ethanol to 3.6 g of $AlCl_3.6H_2O$ gradually in a 250 ml conical flask under magnetic stirring. After that, an ammonia solution of 28% was dropped until the gel was formed under continuous stirring for 3 min. The gel could maturate for 30 hrs at room temperature and then the gel was dried at 100 °C for 24 hrs in the oven. The formed gel was calcined for 2 hrs at 1000°C with a heating rate of 20 °C / min. Finally, $Al_2O_3$ NPS was formed. For preparing capped $Al_2O_3$ NPS with L-methionine, the same procedure above was carried out by adding 0.1 g of L-methionine as a capping agent to the $AlCl_3$ solution. The mechanism of formation of $Al_2O_3$ NPs can be explained by hydrolysis of the aluminum chloride hexahydrate to produce the solution in the presence of ethanol, and then capping agent added before the condensation of hydroxide groups that aggregate together to produce the gel [21].

## 3. Characterization Techniques

The structural identifications and the surface modification of L-methionine capped $Al_2O_3$ NPs and pure $Al_2O_3$ ANPs were characterized by Fourier transform infrared (FTIR) spectrophotometer (Spectrum BX 11- LX 18-5255 Perkin Elmer). The samples were mixed with KBr and this powder were pressed to form a translucent pellet. The spectra were recorded in the wave number range of 4000-400 $cm^{-1}$. The crystalline

DOI: 10.62184/in.jin010120241

Research Article

structures of the prepared materials were evaluated by XRD analysis (X-ray 7000 Shimadzu-Japan) at room temperature. The Bragg angle (2θ) in the range from 5 to 80 degrees was varied to determine the degree of crystallinity of the prepared samples. The X-ray source was Cu target generated at 30 kV and 30 mA with a scan speed of 4deg/min. The microstructure was investigated using (HR-TEM), JEM-2100. Samples were prepared by dispersing 5 mg of a powder sample in 5 ml of ethanol and sonicated for 10 min. A drop of this colloidal solution was evaporated on a copper grid, which was coated with carbon and investigated. The charge of the prepared materials was measured using a Zetasizer Malvern Nano-ZS. The suspension was placed in a universal folded capillary cell attached to platinum electrodes.

## 4. The Measurements of Hydrogen Production

The generation of hydrogen gas from $Al_2O_3$ NPs and capped $Al_2O_3$ NPs was measured using two different techniques under dark and illumination. The system consists of a hot plate, condenser, and flask. The first method was adapted from the work of Rosenband and Gany [19, 20]. The hydrogen gas released was passed through a condenser and then measured in an inverted burette by water displacement. The second method is applied by using a hydrogen sensor. The hydrogen sensor module was prepared by coding the Arduino microcontroller, which is utilized to measure the hydrogen in parts per million (ppm). Arduino Uno R3 is the microcontroller programmed to be used as a medium of interaction by receiving input from the hydrogen sensor module and sending output to the laptop for data recording purposes. The coding commands Arduino to display the hydrogen reading in ppm every second. A hydrogen-harvesting jar was built by attaching the MQ-8 hydrogen sensor module, the hydrogen sensor just below the cover, and the Arduino Uno R3 on the top. Then, all the holes of the cover were sealed with hot glue to ensure the most precise reading of hydrogen. This sensitive hydrogen sensor module which can measure from 10 to 1000 ppm is responsible for detecting the hydrogen produced in the hydrogen jar. The produced amount of hydrogen gas value is only taken once the readings from the hydrogen sensor are found to be in a steady state condition. Another setup measurement system was used to estimate the hydrogen evolved by the hydrogen sensor MQ-8-Arduino Uno R3 controller connected to the laptop. The hydrogen sensor is utilized to measure hydrogen in the range from 10 to 10000 ppm [22]. The hydrogen reading is displayed in ppm every second by Arduino coding. The produced amount of hydrogen gas value is only taken once the readings from the hydrogen sensor are found to be in stable condition as a part of the calibration process. This technique was adopted by the work of Miskon, Thanakodi, Shiema, and Tawil [23].

## 5. Results and Discussion

### 5.1. Structural analysis

The FTIR spectra of the $Al_2O_3$ NPs and capped $Al_2O_3$ with L-methionine are shown in Figure1. The two spectra nearly have the same absorption peaks. The broad and smooth absorption band in the wavenumber range from 500-1000 $cm^{-1}$ reveals the formation of alumina at 567 $cm^{-1}$ represents the Al-O-Al bond and the peak recorded at 754 $cm^{-1}$ is due to the stretching vibration of Al-O. The absorption band around 1638 $cm^{-1}$ indicates the bending mode of water molecules which agreed with the presence of the OH group in the prepared samples [24]. The small absorption peak observed at 2369 $cm^{-1}$ is probably owing to the CN stretching. This band has been formed due to the reaction of ethanol and $NH_3$. The broad absorption band at 3426 $cm^{-1}$ is characteristic of the stretching vibration of the hydroxylates (O-H) group that is bonded to $Al^{3+}$. The absorption peak presented at 1388 $cm^{-1}$ confirms that there are slight changes in the surface chemistry of $Al_2O_3$ when the capping agent of L-methionine was added. This band indicates that the surface binding of $Al_2O_3$ NPs capped with L-methionine is

Integrated Nano, 2024, Vol. XX, No.XX
DOI: 10.62184/in.jin010120241

Research Article

formed via the $NH_2$ group and it is accepted by Alam [24].

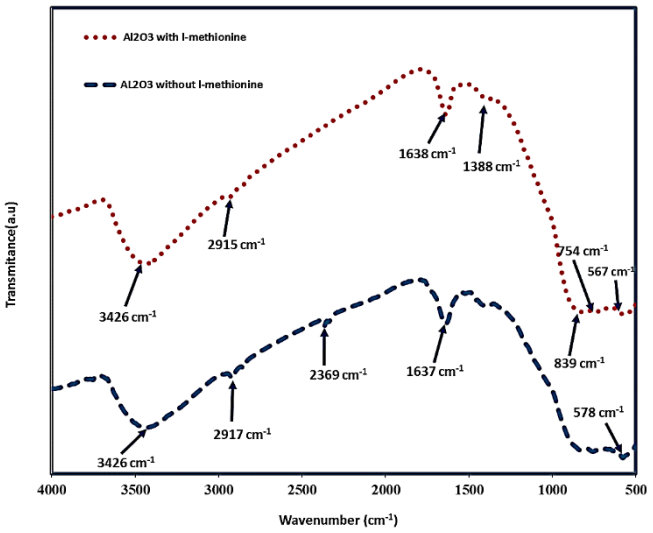


**Figure 1.** FTIR spectra of $Al_2O_3$ NPs and capped $Al_2O_3$.

The XRD patterns of the $Al_2O_3$ NPs and capped $Al_2O_3$ shown in Figure 2 are analyzed to determine the crystallinity. Fig. 2a the pattern of capped $Al_2O_3$ NPs which is highly crystalline and is in great agreement with the XRD pattern of the pure α- $Al_2O_3$ NPs and γ- $Al_2O_3$ NPs powder obtained in a previous work [25, 26]. X-ray patterns of α-$Al_2O_3$ NPs with major peaks at 24.8º, 34.5°, 37°, 42.6°, 52°, 56.8°, and 66°, respectively attributed to the (111), (122), (113), (132), (015,) (134), and (060) diffractions. But the peaks of γ-$Al_2O_3$ NPs are observed at 2θ values 32.16°, 44.7°, and 76.5° correspond to the diffraction planes of (013), (212), and (253), respectively.

Figure 2b shows the XRD pattern of pure $Al_2O_3$ NPs leads to the formation of a mixture of α- and γ- alumina. γ- alumina formation is due to progressive dehydration and surface hydroxyl group desorption and the distorted spinel structure base this phase [27, 28]. The peaks are broad, and profiles are diffused indicating the presence of small crystalline grains and compositional fluctuations. This is consistent with the location of the $Al^{3+}$ ions either by the tetrahedral or octahedral sites within the spinel structure [29]. The α-$Al_2O_3$ NPs diffractions planes appear on the patterns at the 2θ values 34.3°, 42.6°, and 66.4° at (013), (132), and (330), respectively. at The γ-$Al_2O_3$ NPs diffraction planes appear on the patterns at the 2θ values: 44.6° and 56.7° at (122) and (051) respectively [30]. This indicates the alumina is in the form of an alpha-alumina single-phase (cubic structure) with characteristic peaks at 2 θ equal to 32.8°, 37.0°, 39.6°, 45.3°, 46.7°, 60.9°, and 67.4°.

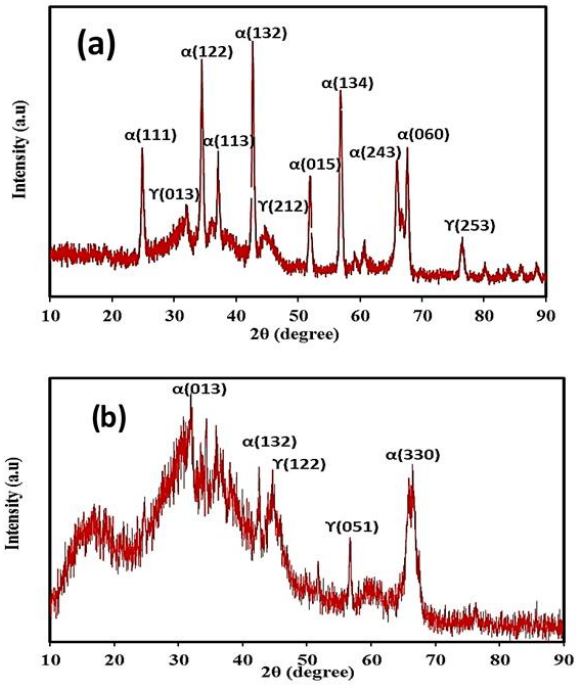


**Figure 2.** XRD pattern of $Al_2O_3$ NPs with (a) capped $Al_2O_3$ NPs and (b) $Al_2O_3$ NPs.

## 5.2. Morphological Properties

As shown in the HRTEM images in Figure 3. The prepared pure $Al_2O_3$ NPs show a lot of aggregations and a high degree of crystallinity as shown in Figure 3a. The particle average sizes of $Al_2O_3$ NPs were 20 nm. Figure 3b shows the HRTEM of capped $Al_2O_3$ NPs which indicates that the spherical-shaped particles formed are homogenous and have less aggregation because of the proper coverage due to the capping agent proper coverage during the nucleation initial stages which prevents the particles from coarsening. The particle average size of capped $Al_2O_3$ NPs with L-methionine was 13 nm [30].

Integrated Nano, 2024, Vol. XX, No.XX

DOI: 10.62184/in.jin010120241

Research Article

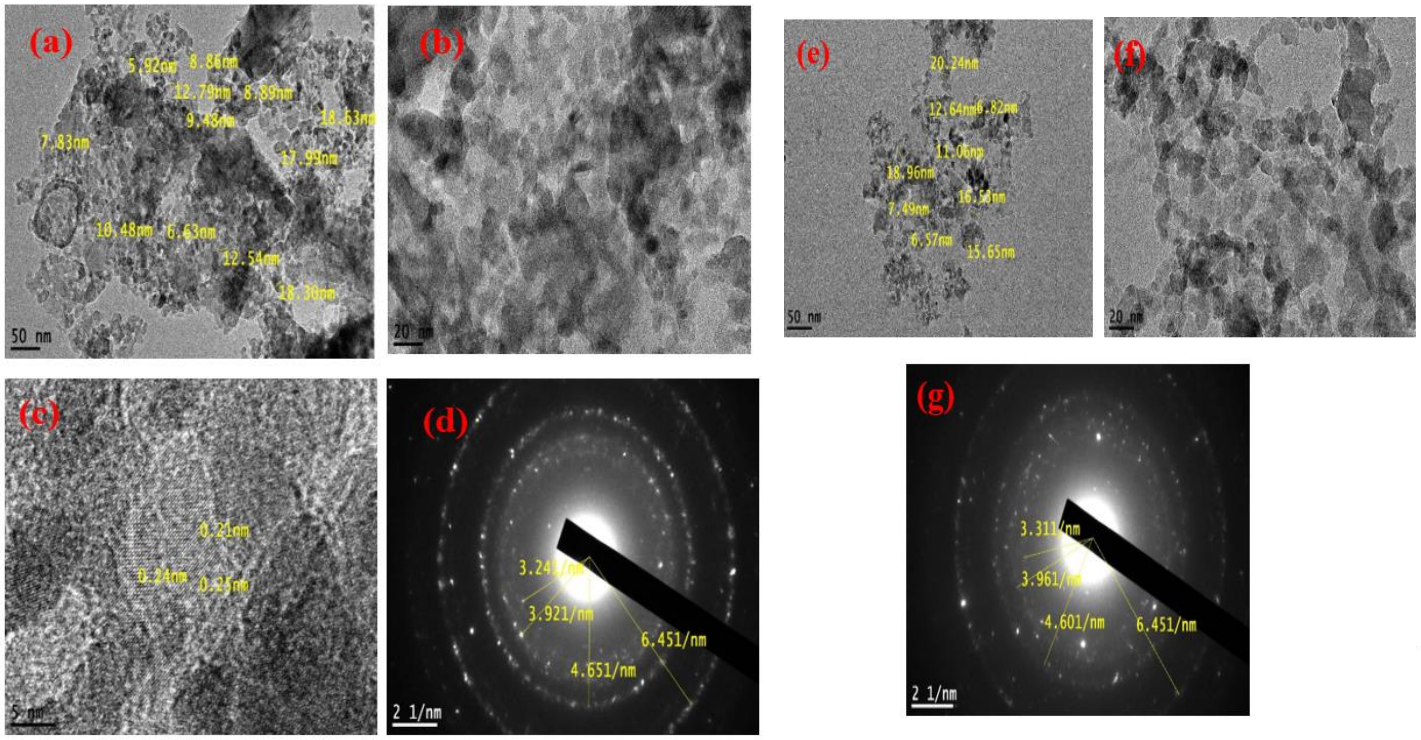


**Figure 3.** HRTEM image and SEAD of pure $Al_2O_3$ NPs (a, b, c and d) capped $Al_2O_3$ NPs with L- methionine (e, f, and g).

The Zeta potential of capped $Al_2O_3$ NPs with L-methionine equals - 24.5 mV. The particles' surface charge is completely negative which means more stable. The electrostatic stability of suspension is due to strong repulsive force which reduces coalescing probability among particle charges which makes the suspension more stable in the alkaline media. This is in good agreement with the work of Zawrah [30]. The Zeta potential of pure $Al_2O_3$ NPs equals - 21.4 mV and it is less stable than capped $Al_2O_3$ NPs.

## 5.3. Photocatalytic Activity

Figure 4 presents the different concentration effects of capped $Al_2O_3$ NPs with L- methionine (0.1, 0.2, 0.3, and 0.4 g) suspended in 50 ml $H_2O$ under indoor natural light for 30 min at 75°C at a pH of 7.5 on the hydrogen evolved and measured by burette. It is noted that after 30 min, the values of hydrogen evolved from 0.1, 0.2, 0.3, and 0.4 g were 60.5, 60, 36.5, and 20.5 ml, respectively. The rate of the reaction depends on the capped $Al_2O_3$ NP concentrations [23]. The rates of hydrogen revolved from 0.1, 0.2, and 0.4 g were 2.02, 2.07, and 0.7 ml/min, respectively. The rates of hydrogen revolved from 0.3 g were 1.9, and 0.88 ml/min, respectively. The rate of hydrogen evolved from 0.2 g is the highest yield especially after 15 min due to its low concentration which increases specific surface and makes the reaction faster as shown in Figure 4 [17]. The hydrolysis process that occurred can be expressed as shown in the following equations 1 and 2 [30]:

$$Al_2O_3 + H_2O \rightarrow 2\,AlOOH \quad (1)$$

$$AlOOH \rightarrow Al_2O_3 + 1/2O_2 + H_2 \quad (2)$$

Figure 5 compares the hydrogen evolved from a concentration of 0.2 g of capped $Al_2O_3$ NPs with L- methionine and pure $Al_2O_3$ NPs suspended in 50 ml $H_2O$ under indoor natural light for 30 min at 75 °C at and pH of 7.5. It is noticed

Integrated Nano, 2024, Vol. XX, No.XX
DOI: 10.62184/in.jin010120241

Research Article

that after 5 min capped $Al_2O_3$ NPs have the same yield as pure $Al_2O_3$ NPs. It is noted that there are two rates of reaction. These rates of hydrogen evolved from capped $Al_2O_3$ NPs are 3.5 and 0.47 ml/min, respectively. However, the rates of hydrogen evolved from pure $Al_2O_3$ NPs are 2.75 and 0.82 ml/min, respectively. The effect of the capping agent on the hydrogen evolved improving the particles to become finer, less agglomerated, and more uniform as presented in HRTEM in Figure3.

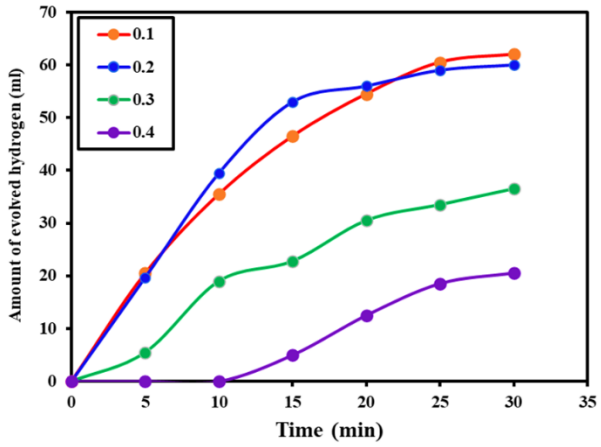


**Figure 4.** Amount of hydrogen produced from a different concentration of capped $Al_2O_3$ NPs with L-methionine.

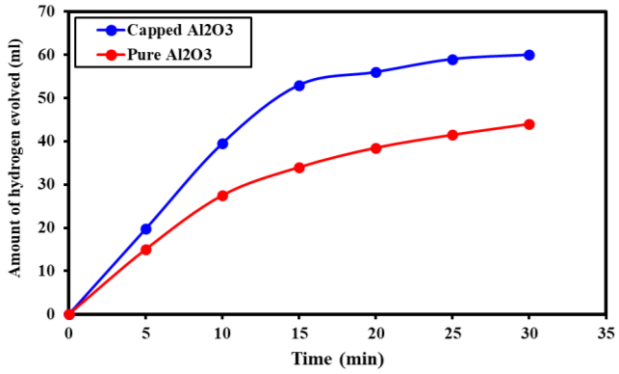


**Figure 5.** Amount of hydrogen produced from 0.2 g of pure and capped $Al_2O_3$ NPs.

The hydrogen evolved amounts from 0.2 g of capped $Al_2O_3$ NPs with L- methionine suspended in 50 ml $H_2O$ under indoor natural light and dark for 25 min at 75° C and pH of 7.5 are shown in Figure 6. The rates of the amount of evolved hydrogen of capped $Al_2O_3$ NPs under indoor natural light and dark were 2.5 and 2.4 ml/min, respectively. When the temperature of 75° C was used under indoor natural light and dark, it was observed that the rate of evolved hydrogen under indoor natural light was nearly the same as under dark. As a result of the presence of visible light, a little acceleration of the reaction observed. It can be concluded that this reaction is independent of light. This result is in agreement with the work performed by Deng [30].

Figure 7 presents the amount of hydrogen evolved from 0.2 g of capped $Al_2O_3$ NPs with L- methionine suspended in 50 ml $H_2O$ under indoor natural light for 40 min at 75° C and pH of 7.5 measured using hydrogen sensor. From the figure, the maximum peak appeared at 866 ppm after 9.5 min. This result is in good agreement with the work performed by Miskon [22].

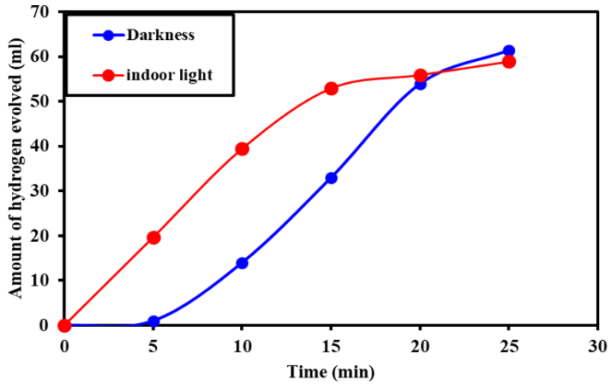


**Figure 6.** Amount of hydrogen produced from 0.2 g of $Al_2O_3$ NPs under indoor natural light and dark.

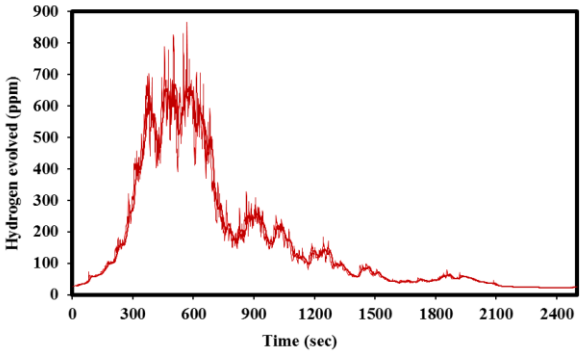


**Figure 7.** Amount of hydrogen sensed from 0.2 g of $Al_2O_3$ NPs using hydrogen sensor.

DOI: 10.62184/in.jin010120241

Research Article

## 6. Conclusions

$Al_2O_3$ NPs used as a photocatalyst in the production of hydrogen under illumination and darkness. The prepared $Al_2O_3$ NPs were polycrystalline, and the particle average sizes of capped $Al_2O_3$ NPs with L-methionine were 13 nm and pure was 20 nm. Capped $Al_2O_3$ NPs had higher stability and yield compared to pure $Al_2O_3$ NPs, due to the presence of a capping agent which improved the stability of $Al_2O_3$ NPs in the production of hydrogen. The highest yield of evolved hydrogen was 60 ml with evolved rate of 2.07 ml/min at 75 °C at a pH of 7.5 after 30 min.

## Declaration of interest statement

The authors declare that this work has not been done or published before and has no competing financial interests.

## Author contributions

Mai Medhat and Marwa Khalil contributed to ideas, experiment execution, interpretation of the data, and writing of the manuscript. Ahmed M. Elshaer contributed to the experiment execution, Moataz Soliman and Shaker Ebrahim supervised, wrote, and edited the manuscript.

## Author Information

**Corresponding Author:** Marwa Khalil*

**E-mail:** igsr.Marwa.khalil@alexu.edu.eg

**ORCID**: https://orcid.org/0000-0002-7948-7231

## References

[1] Kannah, R.Y., Kavitha, S., Preethi, Karthikeyan, O.P., Kumar, G., Dai-Viet, N.V., and Banu, J.R. (2021). Techno-economic assessment of various hydrogen production methods-A review. Bioresource technology, 319, 124175, http://doi.org/10.1016/j.biortech.2020.124175.

[2] Jain, N., Sangwa, N.R., Kumar, K., Sharma, A., and Mathur, Y.B. (2020). Energy crisis, resource scarcity, and innovations in biofuels. Journal of Advanced Research in Alternative Energy, Environment and Ecology,7, 4, http://doi.org/10.24321/2455.3093.202007.

[3] Zhang, B., Zhang, S.-X., Yao, R., Wu, Y.-H., and Qiu, J.-S. (2021). Progress and prospects of hydrogen production: Opportunities and challenges. Journal of Electronic Science and Technology, 19, 100080, https://doi.org/10.1016/j.jnlest.2021.100080.

[4] Wang, S., Lu, A., and Zhong, C.-J. (2021). Hydrogen production from water electrolysis: Role of catalysts. Nano Convergence, 8, 1, https://doi.org/10.1186/s40580-021-00254-x.

[5] Nishiyama, H., Yamada, T., Nakabayashi, M., Maehara, Y., Yamaguchi, M., and Kuromiya, Y. et al. (2021). Photocatalytic solar hydrogen production from water on a 100 $m^2$-scale. Nature, 598, 304, https://doi.org/10.1038/s41586-021-03907-3.

[6] Sherif, S.A., Barbir, F., and Veziroglu, T.N. (2003). Principles of hydrogen energy production, storage and utilization. Journal of Scientific & Industrial Research, 62, 46. https://doi.org/10.1016/S0140-6701(04)91346-X.

[7] Commission, E.-E. (2003). Hydrogen energy and fuel cells-a vision of n our future. Final report of the High Level Group. EUR. 37, 37121708, https://doi.org/10.1016/S1464-2859(03)00729-6.

[8] Riis, T., Hagen, E.F., Vie, P.J., and Ulleberg, Ø. (2005). Hydrogen production–gaps and priorities. IEA Hydrogen Implementing Agreement (IEA, Paris, 2005), 1. https://api.semanticscholar.org/CorpusID:204894629.

[9] Martino, M., Ruocco, C., Meloni, E., Pullumbi P., and Palma, V. (2021). Main hydrogen production processes: An overview. Catalysts, 11, 547, https://doi.org/10.3390/catal11050547.

[10] Tentu, R.D., and Basu, S. (2017). Photocatalytic water splitting for hydrogen production. Current Opinion in Electrochemistry, 5, 56, https://doi.org/10.1016/j.coelec.2017.10.019.

[11] Rashid, M., Al Mesfer, M.K. Naseem, H., and Danish, M. (2015). Hydrogen production by water electrolysis: a review of alkaline water electrolysis, PEM water electrolysis and high temperature water electrolysis. International Journal of Engineering and Advanced Technology, 4, 1, https://doi.org/10.35940/ijeat.2249-8958.

[12] Maeda, K., (2011). Photocatalytic water splitting using semiconductor particles: history and recent developments. Journal of Photochemistry and Photobiology C: Photochemistry Reviews, 12, 237, https://doi.org/10.1016/j.jphotochemrev.2011.07.001.

[13] Hall, D.O., and Palz, W. (1982) Photochemical, photoelectrochemical and photobiological processes. 7666, Springer Science & Business Media.

DOI: 10.62184/in.jin010120241



[14] Zhao, Y., Hoivik, N., and Wang, K. **(**2016). Recent advance on engineering titanium dioxide nanotubes for photochemical and photoelectrochemical water splitting. Nano energy, 30, 728, https://doi.org/10.1016/j.nanoen.2016.09.027.

[15] Chen, Z., Dinh, H.N., and Miller, E. (2013). Photoelectrochemical water splitting. 344, https://doi.org/10.1007/978-1-4614-8298-7 .

[16] Baudín, C., (2014). Processing of alumina and corresponding composites, https://doi.org/10.1016/B978-0-08-096527-7.00021-0

[17] Rogojan, R., Andronescu, E. Ghitulica, C., and Vasile, B.S. (2011). Synthesis and characterization of alumina nano-powder obtained by sol-gel method. UPB Buletin Stiintific, Series B: Chemistry and Materials Science, 73, 67, ISSN 1454-2331

[18] Eidsvåg, H., Bentouba,S. Vajeeston, P. Yohi, S., and Velauthapillai, D. (2021). $TiO_2$ as a photocatalyst for water splitting—an experimental and theoretical review. Molecules, 26, 1687 https://doi.org/10.3390/molecules26061687

[19] Singh, S.B., (2021). Nanomaterials for water splitting: a greener approach to generate hydrogen. handbook of nanomaterials and nanocomposites for energy and environmental applications, 1201, https://doi.org/10.1007/978-3-030-36268-3_32

[20] Rosenband, V., and Gany, A. (2010). Application of activated aluminum powder for generation of hydrogen from water. International Journal of Hydrogen Energy, 35, 10898,

https://doi.org/10.1016/j.ijhydene.2010.07.019.

[21] Sifontes, Á.B., Gutierrez, B., Mónaco, A., Yanez, A., Díaz, Y., Méndez, F.J., Llovera, L., Cañizales, E., and Brito, J.L. (2014). Preparation of functionalized porous nano-γ- $Al_2O_3$ powders employing colophony extract. Biotechnology Reports, 4, 21,

https://doi.org/10.1016/j.btre.2014.07.001.

[22] Miskon, A., Thanakodi, Shiema, N., Chong, M.W.K., Takriff, M.S., Kamarudin, K.F., Norzali, A., and Tawil, S.N.M. (2016). Feasibility studies of vortex flow impact on the proliferation of algae in hydrogen production for fuel cell applications. IOP Conference Series: Materials Science and Engineering, 160, 012092 https://doi.org/10.1088/1757-899X/160/1/012092.

[23] Lashanizadegan, M., Farzi, G., and Nia, N.E. (2014). Synthesis and surface modification of aluminum oxide nanoparticles. Journal of Ceramic Processing Research, 15, 316.

[24] Alam, S.N., Kumar, L., and Sahoo, A.R. (2016). Comparison of α- $Al_2O_3$ synthesized by sol-gel process using $AlCl_3$ andal $(NO_3)_3$ as precursors. Nano Material Nano Composites.

[25] Saud, A., Majdi, H.S., and Saud, S. (2019). Synthesis of nano-alumina powder via recrystallization of ammonium alum. Cerâmica, 65, 236, https://doi.org/10.1590/0366-69132019653742636

[26] Zawrah, M., Khattab, R., Girgis, L., El Daidamony, H., and Abdel Aziz, R.E. (2016).Stability and electrical conductivity of water-base $Al_2O_3$ nanofluids for different applications. HBRC journal, 12, 227, https://doi.org/10.1016/j.hbrcj.2014.12.001.

[27] Cava, S., Tebcherani, S.M., Souza, I.A., Pianaro, S.A., Paskocimas, C.A., Longo, E., and Varela, J.A. (2007) Structural characterization of phase transition of $Al_2O_3$ nanopowders obtained by polymeric precursor method. Materials Chemistry and Physics, 103, 394, https://doi.org/10.1016/j.matchemphys.2007.02.046.

[28] Branch, M. (2011). Preparation of nano-scale α-$Al_2O_3$ powder by the sol-gel method. Ceramics–Silikáty, 55 (4), 378.

[29] Petrovic, J., and Thomas, G (2011). Reaction of aluminum with water to produce hydrogen-2010 update., Office of Energy Efficiency and Renewable Energy, https://doi.org/10.2172/1219359.

[30] Deng, Z.Y., Liu.,Y. Tanaka,Y., Zhang, H.W., Ye, J., and Kagawa, Y. (2005). Temperature effect on hydrogen generation by the reaction of γ-$Al_2O_3$-modified Al powder with distilled water. Journal of the American Ceramic Society, 88, 2975, https://doi.org/10.1016/j.btre.2014.07.001.